

# On the possibility of rogue wave generation based on the dynamics of modified Burridge-Knopoff model of earthquake fault

Nkeh Oma Nfor<sup>\*,1</sup>, Ndikum Eric Ndoh<sup>1</sup>, Marceline Motchongom Tingue<sup>2</sup>  
and Vivian Ndfutu Nfor<sup>2</sup>

<sup>(1)</sup>Department of Physics, Higher Teacher Training College Bambili, The University of Bamenda, P. O. Box 39, Bambili-Cameroon

<sup>(2)</sup>Department of Fundamental Science, Higher Technical Teacher Training College Bambili, The University of Bamenda, P. O. Box 39, Bambili-Cameroon

Article history: received May 30, 2022; accepted October 21, 2022

## Abstract

In this study we propose a modified Burridge-Knopoff model of earthquake fault, in which two tectonic plates are strongly coupled by nonlinear springs. By minimizing the effects of the velocity-weakening stick-slip friction force between the masses and the moving surface, and in the limit of low amplitude oscillations; the system exhibits both stick-slip and damped oscillatory motions as the values of some parameters are varied. Such motions usually characterize the dynamics of an earthquake fault, even though it is not always felt because of the low amplitude of vibrations. However when enough stress builds up in the subduction zones to overcome the frictional forces between tectonic plates, the oceanic rocks suddenly slip and there is violent release of energy at the epicentre. This outburst of energy simply signifies the generation of a very large amplitude and localized nonlinear wave. Such wave profile exactly fits the Peregrine solution of the damped/forced nonlinear Schrodinger amplitude equation, derived from the modified one-dimensional Burridge-Knopoff equation of motion. In the regime of minimal or no frictional forces, these monster waves suddenly appear and disappear without traces as shown by the numerical investigations. Our results strongly suggest that rogue waves emanates from the dynamics of nonlinearly coupled tectonic plates in subduction zones. This is further complemented by the fact that these giant waves were initially observed in Pacific and Atlantic oceans, which play hosts to the world's largest oceanic subduction zones.

Keywords: Burridge-Knopoff; Model; Tectonic plates; Stick-slip friction; Rogue waves

---

## 1. Introduction

Geographical locations in the world which are vulnerable to seismic activities have suffered huge damages during the occurrence of earthquakes. Numerous research activities in the previous decades are focused on obtaining

reliable data for the prediction of earthquake phenomena. From a mechanical standpoint, pioneer models proposed by Burridge and Knopoff (BK) provide valuable information that depicts real seismic activities which satisfy the Gutenberg-Richter statistics [Burridge and Knopoff, 1967; Carlson and Langer, 1989a; Carlson and Langer, 1989b; Carlson et al., 1991; Carlson et al., 1994]. However, new technological advancement in seismology and geodesy has significantly enhanced our knowledge on the dynamics of related earthquake processes, which are useful tools in the mitigation of seismic risks. It should be noted that hazard is the intrinsic natural occurrence of earthquakes and the resulting ground motion and other effects, while the risk is the danger the hazard poses to life and property. Hence it is clear that research activities by scientists on earth is limited in the face of geological hazards, but has gone a long way to minimize the risks by furnishing the population with appropriate information.

Large amplitude oscillation which emanates from vibrating mechanical systems has led to destructive tsunamis and rogue waves [Kharif et al. 2009]. Tsunami waves are principally generated by earthquakes, even though submarine and coastal landslides can ignite more intense tsunami wave profiles. The so-called rogue waves are very large-amplitude waves that appears on the sea surface and pose great threats to maritime structures [Kharif et al., 2009; Dysthe et al., 2008; Adcock and Taylor, 2014; Nikolkina and Didenkulova, 2014; Mori et al. 2002]. A glaring example is the collision between huge ships and rogue waves that let to enormous human and material losses as reported in *New Scientist Magazine* [Lawton, 2001]. Consequently, numerous research activities have been oriented toward understanding the physics of huge wave appearance and its interaction with the immediate environment. Memories of the event where the 56-foot research vessel R/V Ballena capsized in a rogue wave south of Point Arguello, California on November 4, 2000 is still very fresh in our minds [Graham, 2000]. Even though rogue waves were initially identified within the context of maritime environment, numerous studies have already been carried out to extend it to the fields of non-linear optics [Estelle and Kofane', 2015; Solli et al., 2007; Dudley et al., 2014; Akhmediev et al., 2016] and Bose-Einstein condensation [Zhong et al., 2015]. Rogue waves have also been experimentally realized in plasmas [Bailung et al. 2011], super fluid Helium [Ganshin et al. 2008], and transport in microwave systems [Hohmann et al. 2010], and parametrically driven capillary waves [Shats and Punzmann, 2010]. Motivated by this ubiquitous nature of rogue waves with the ability of being experimentally generated, this study seeks to analytically and numerically demonstrate the inextricable link between rogue wave generation and earthquake occurrence.

Intense studies in the 1960s which focused on tectonic plate theory, accompanied by a thriving of seismology and experimental rock mechanics, and stick-slip instabilities along pre-existing discontinuities (i.e. tectonic faults) are increasingly being exploited as the most prominent earthquake mechanism [Brace and Byerlee, 1966; Byerlee, 1970]. The relative movement of the earth's tectonic plates is a process driven by the thermal activity of the inner earth. Different mechanisms of relative plate movement occur, resulting to different degrees of destruction; with the most destructive effect induced in regions where tectonic plates move tangentially to each other. The zones showing the latter configuration are called subduction zones [Lallemand, 2014]. The world's largest subduction zones can be traced at the borders of the pacific plate, including the coasts of Chile, California, Japan, and the Philippines. The mechanical analysis of earthquake processes is generally categorized into two main approaches. The first conceives earthquakes as fracture activities and therefore stresses on the investigation of brittle and ductile fracture of rocks and the shear behaviour of granular media. In this active domain of research investigation, there are a plethora of studies as reflected in [Baro et al., 2013; Main, 2013; Ben-Zion and Sammis, 2011; Hamiel et al., 2009]. This approach is particularly relevant for deep earthquake events triggered by very high pressure activities. On the other hand, Brace et. al. rigorously demonstrated in 1966 that shallow earthquakes are not to be considered as fracture phenomena because the prevailing normal pressures are much smaller [Brace and Byerlee, 1966]. They went further by interpreting shallow earthquakes as stick-slip instabilities, characterized as a purely friction phenomenon. In fact stick-slip is not only limited to earthquake dynamics, but in a broad spectrum of mechanical systems in which dynamic frictional contacts are present; leading to alternation between sticking and slipping motions.

The original BK model clearly captures earthquake fault dynamics, in which the interaction of two tectonic plates in a geological fault is modelled as a chain of blocks elastically coupled together [Burridge and Knopoff, 1967]. In the model, one of the plates is subjected to a friction force by the surface of the other plate, thereby inducing stick-slip motion. The model provided the basis for understanding the mechanisms of Gutenberg-Richter scaling and the relation between large and small events. In reference [Carlson and Langer, 1989a], Carlson et al. investigated on the dynamic behaviour of the BK model with the velocity-weakening stick-slip friction force between the masses and the moving surface being the only non-linearity introduced into the system. The system was shown to exhibit noisy sequences of earthquake-like events after being consistently driven toward a slipping

instability. The authors went further in their subsequent studies and presented a comprehensive numerical analysis of certain intrinsic properties of the one-dimensional homogeneous BK model. It was revealed that the magnitude distribution of smaller events is consistent with the Gutenberg-Richter law, while the larger events occur in excess of this distribution [Carlson et al., 1991].

Unlike previous studies where nonlinearity is only introduced by the velocity-weakening stick-slip friction force between the masses and the moving surface [Burridge and Knopoff, 1967; Carlson et al., 1994], the current investigation further explores additional non-linearity induced in the system. We consider the dynamics of the block and spring system of the modified BK model, in which there exists very strong interaction between the two tectonic plates [Nkomom et al., 2021; Akishin et al., 2000; Pelap et al., 2016]. These interactions are modelled by nonlinear springs (i.e. a hardening or softening spring whose spring constant is dependent on the displacement between the plates). With this configuration, harmonic oscillations in the absence of frictional forces can only be observed at very low block displacements. This study seeks to elucidate on the origin of oceanic rogue waves, which is a subject matter still under intense debate among scientists [Akhmediev and Pelinovsky, 2010]. It should be noted that nonlinear effects are well-known in springs when there is high relative displacement in the direction of motion [Nkomom et al., 2021; Akishin et al., 2000; Pelap et al., 2016; Wiggins, 1990; Enns, 2011]. The anharmonic inter-plate interaction is more realistic because it ensures small amplitude of block displacements and velocities, and gives us the opportunity to explain new patterns in the mechanical system. Consequently, only very strong external perturbations can disrupt the frictional forces between plates in order to trigger an earthquake.

The present paper is organized as follows. In section 2 we present the modified one-dimensional BK model and derive the appropriate equations using the continuum limit approximations with various dimensionless parameters. Analysis in section 3 is limited to oscillations in the linear regime, where the displacement and velocity profiles of the system are obtained under appropriate conditions. When the nonlinear parameter is fully considered in section 4, we explore the method of multiple scale analysis to obtain the damped/forced nonlinear Schrodinger amplitude equation. Solutions of this amplitude equation clearly demonstrate that the dynamics of nonlinearly coupled tectonic plates in subduction zones may be responsible for the generation of oceanic rogue waves as highlighted in the numerical analysis. Various profiles of the rogue waves which corresponds to different magnitude of destructions are obtained with the change of system parameters. Finally, section 5 summarizes the results obtained and give other important perspectives.

## 2. Model equations

We consider a modified BK model which consists of blocks connected by linear springs to their nearest neighbours; with spring constant  $K_c$  as represented in Figure 1. The blocks are also connected to a loader plate by nonlinear springs with spring constant  $K_p(x_n)$ , and rest on a surface with a nonlinear velocity-weakening stick-slip friction

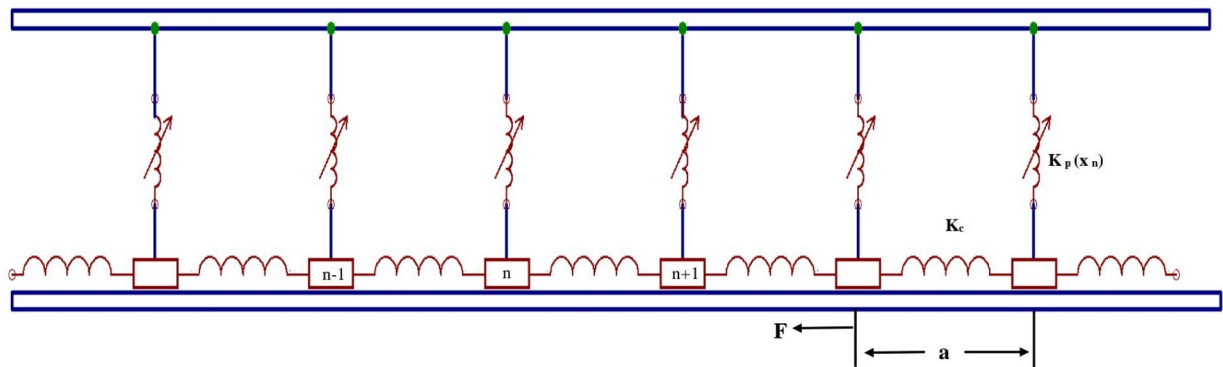


**Figure 1.** Mechanical interpretation of block and spring system for the modified BK model. The system is assume to be spatially homogeneous and consists of equal masses  $m$ , which are linearly connected to nearest neighbours by springs of strength  $K_c$  and to a stationary upper surface by nonlinear springs of strength  $K_p(x_n)$ . Each mass experiences a frictional force  $F(x)$ , which is a function of only the velocity of the block.

force that depends on a parameter  $\alpha$ . This parameter controls how quickly the friction force decreases as the velocity is increased, and determines the amount of stress dissipated in an event. The blocks are fundamentally conceived as the points of contact between the two plates along a lateral fault, and moving at speed  $v$  relative to each other.

The equations of motion of the modified BK model can be shown to be [Carlson and Langer, 1989a; Carlson and Langer, 1989b]

$$m\ddot{x}_n = K_c(x_{n+1} - 2x_n + x_{n-1}) - K_p(x_n)x_n - F(v + \dot{x}_n), \quad (1)$$

where

$$K_p(x_n) = K_0 \left[ 1 + \frac{K_\beta}{K_0} x_n^2 \right], \quad (2)$$

is the nonlinear strength of torsional elements which models the strong interaction between the two tectonic plates [Nkomom et al., 2021; Akishin et al., 2000; Pelap et al., 2016]. The nature of coupling between two tectonic plates is an important parameter used to determine the magnitude of seismic hazards. It is important to note that a hardening nonlinear spring is one whose strength gradually increases when progressively subjected to increased extension or compression i.e. the spring provides a progressively hardening reaction as the spring gets extended or compressed [Wiggins, 1990; Enns, 2011]. On the other hand, a softening nonlinear spring gradually decreases its spring rate as the spring is subjected to an increased deflection. The relationship between the nonlinear spring constant  $K_p(x_n)$  and displacement  $x_n$  is depicted in Figure 2 for both hardening and softening springs. In the regime where  $K_\beta/K_0 \approx 1$  for a hardening spring as shown in Figure 2(a), we observe a very interesting phenomenon in which the strength of the torsional spring constant increases quadratically with the displacement  $x_n$ . In fact, when  $K_\beta$  varies from 0.70 to 1.00, large displacements induces high coupling strengths between tectonic plates in the mechanical configuration of the system. However for  $K_\beta/K_0 \ll 1$  as with the case for  $K_\beta = 0.00, 0.03, 0.05$  in Figure 2(a), it implies  $K_p(x_n) \approx K_0$  as reflected in numerous studies carried out [Burridge and Knopoff, 1967; Carlson and Langer, 1989a; Carlson and Langer, 1989b; Carlson et al., 1991; Carlson et al., 1994], where the coupling between tectonic plates is independent of the displacement (linear springs). The corresponding dependence of nonlinear spring strength on displacement for softening springs is shown in Figure 2(b), whose profile is just the reverse of a hardening spring because the spring strength decreases with increase in displacement. For the frictional law  $F$ , we consider a function of the form

$$F(\dot{x}) = F_0 \phi \left( \frac{\dot{x}}{v_1} \right), \quad (3)$$

which is the velocity-dependent friction force and  $v_1$  is a characteristic velocity. As in Ref. [Carlson and Langer, 1989b] we introduce the following parameters given by:  $\tau = \omega_p t$ ,  $\omega_p^2 = \frac{K_0}{m}$ ,  $D_0 = \frac{F_0}{K_0}$  and  $u_n = (K_0/F_0)x_n$ . In these new units, we rewrite equation (1) as

$$\ddot{u}_n = l^2(u_{n+1} - 2u_n + u_{n-1}) - (1 + \gamma u_n^2)u_n - \phi(2\alpha v + 2\alpha \dot{u}_n), \quad (4)$$

where

$$l^2 = \frac{K_c}{K_0}, v = \frac{v}{\omega_p D_0}, 2\alpha = \frac{\omega_p D_0}{v_1}, \gamma = \frac{K_\beta D_0^2}{K_0}. \quad (5)$$

System (4) is a dissipative discrete nonlinear partial differential equation which cannot be solved analytically because of the undefined form of the frictional law. However for  $\gamma = 0$  and imploring spinal frictional laws in this discrete regime, Cartwright et al. showed that at both low and high slipping velocities; the friction function

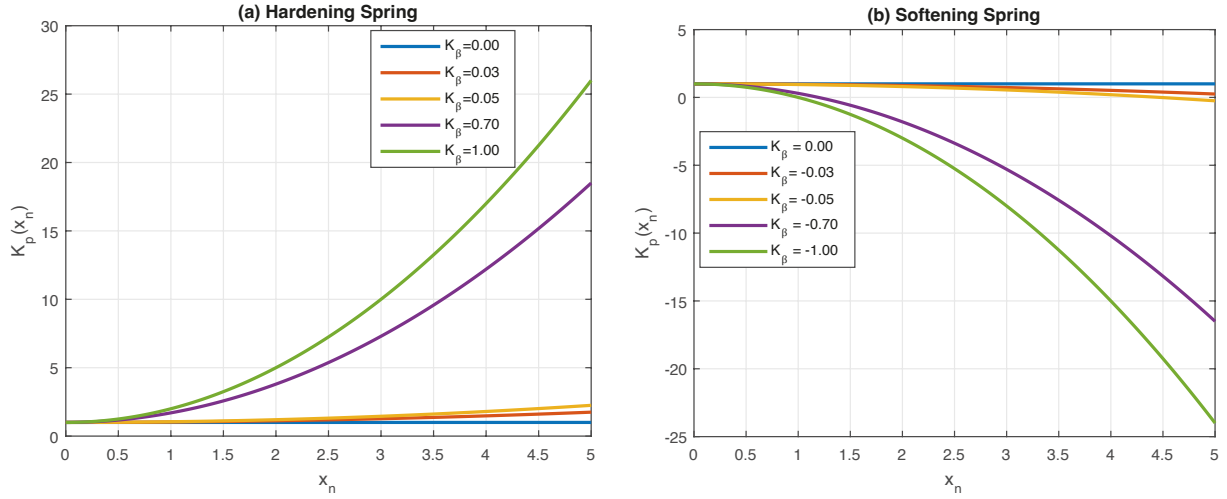


**Figure 2.** Variation of nonlinear spring constant  $K_p(x_n)$  in equation (2), as the value of the parameter  $K_\beta$  is varied and for  $K_0 = 1.00$ .

is velocity-strengthening and velocity-weakening for intermediate slipping velocities [Cartwright et al., 1999]. Morales et al. further reported on the existence of solitary wave solutions in the BK model, with perturbations of the rest state lying above some threshold quickly evolving into a solitary wave [Morales et al., 2018]. The solitary waves fail to propagate and converge towards spatially uniform rest state when subjected to minimal perturbations.

By imposing the continuum limit approximation

$$u_n(t) \rightarrow u(x, t), x = na, u_{n\pm 1} = u \pm a \frac{\partial u}{\partial x} + \frac{a^2}{2} \frac{\partial^2 u}{\partial x^2} + \dots, \quad (6)$$

where  $a$  is the lattice spacing, appropriate solutions of equation (4) can always be obtained. The validity of this approximation is based on the fact that the displacement  $u$  varies slowly from one mass to the other (i.e.  $K_c \gg K_0$ ). Consequently, equation (4) is transformed to

$$\frac{\partial^2 u}{\partial t^2} = a^2 l^2 \frac{\partial^2 u}{\partial x^2} - (1 + \gamma u^2)u - \phi(2av + 2a\dot{u}). \quad (7)$$

The initial form of the friction law proposed by Carlson and Langer is given in its dimensionless form by [Carlson and Langer, 1989b]

$$\phi(x) = \frac{1}{1 + |x|} \text{sgn}(x). \quad (8)$$

This law is characterized by the fact that the zero velocity (i.e.  $\phi(0)$ ) is any value within  $\pm 1$  irrespective of the force required to oppose that of the springs. However, in order for Carlson and Langer to comprehensively study the transition between localized and greater delocalized events, this friction law in (8) was later modified to [Carlson et al., 1991]

$$\phi(x) = \begin{cases} (-\infty, 1], & x = 0 \\ \frac{1 - \sigma}{1 + \frac{x}{1 - \sigma}}, & x > 0. \end{cases} \quad (9)$$

The modified equation (9) clearly shows that for zero velocity, the friction force is constrained within the interval  $(-\infty, 1]$ . Furthermore, the system no longer support negative velocity with the value of the maximum sliding friction force fixed at  $1 - \sigma$  (the parameter  $\sigma$  is the force drop or, equivalently, the acceleration of a block at the instant slipping begins), while the corresponding maximum value of the static frictional force is maintained at unity.

In our current investigation, we focus on the dynamics frictional force (i.e.  $\dot{u} > -v$ ) and assume that  $\alpha\dot{u} \ll 1$ , so that the nonlinear part of the function  $\phi$  is neglected. By setting  $x = 2\alpha v + 2\alpha\dot{u}$  and  $\sigma = 1 - 2\alpha v$  in this linear approximation, equation (7) can now be re-written as [Nkomom et al., 2021; Pelap et al., 2016]

$$\ddot{u} = \alpha^2 l^2 \frac{\partial^2 u}{\partial x^2} - (1 + \gamma u^2)u + 2\alpha\dot{u}. \quad (10)$$

The dissipative effect in equation (10) obeys the Stoke's force law, that is the viscous force is directly proportional to the velocity of the system [Kittel et al., 1968]. From this equation, it is becoming increasingly clear that these damping and nonlinear terms introduced are key ingredients in determining the patterns emanating from two nonlinearly coupled tectonic plates. It is difficult to directly measure the velocity-weakening rate parameter  $\alpha$ , which is an important stability factor that determines the slip complexity of the system. Large magnitude of  $\alpha$  values favours stronger instability and less energy dissipation, while smaller  $\alpha$  means more dissipation and weaker instability [Langer et al., 1996].

### 3. Oscillations in the linear regime

A system of linear differential equations is one for which the dependent quantities or variables only appear to the first power. The superposition principle works perfectly well for linear systems [Enns, 2011]. If terms are present which involve products of the dependent variables, or other powers (or other mathematical forms), the system is therefore regarded as being nonlinear as is the case with equation (10) for  $\gamma \neq 0$ . However in this section, we focus on low amplitude oscillations that characterize harmonic vibrations between tectonic plates for which  $\frac{K_\beta}{K_0} \ll 1$  (i.e.  $\gamma = 0$ ). Consequently we introduce the block displacement in the form of the travelling wave

$$u(x, t) = u(\xi); \quad \xi = x - v_0 t, \quad (11)$$

where  $v_0$  is undetermined parameter that represents the velocity of propagation. A low amplitude propagating mode solution can be obtained by substituting equation (11) into the partial differential equation (10) for  $\gamma = 0$ , to obtain the ordinary differential equation

$$(v_0^2 - \alpha^2 l^2) \frac{d^2 u}{d\xi^2} + (2v_0 \alpha) \frac{du}{d\xi} + u = 0. \quad (12)$$

By considering a trial solution to equation (12) of the form  $u(\xi) = C \exp(i\theta\xi)$ , leads to the quadratic equation

$$(v_0^2 - \alpha^2 l^2)\theta^2 - i(2v_0 \alpha)\theta - 1 = 0, \quad (13)$$

with solution

$$\theta = \frac{iv_0 \alpha}{(v_0^2 - \alpha^2 l^2)} \pm \sqrt{\frac{v_0^2(1 - \alpha^2) - \alpha^2 l^2}{(v_0^2 - \alpha^2 l^2)^2}}. \quad (14)$$

This naturally leads us to obtain solution of the form

$$u(\xi) = C e^{-v_0 \alpha \xi / v_0^2 - a^2 l^2} \exp \left\{ \pm i \left[ \sqrt{\frac{v_0^2 (1 - \alpha^2) - a^2 l^2}{(v_0^2 - a^2 l^2)^2}} \right] \xi \right\}, \quad (15)$$

for  $v_0^2 - a^2 l^2 > 0$  and  $C$  being a constant, in which we now highlight some special cases of this solution.

For  $v_0^2 - a^2 l^2 < v_0^2 \alpha^2$ , we obtain a non-oscillatory solution of the form

$$u(\xi) = A e_0^{-v_0 \alpha \xi / v_0^2 - a^2 l^2} \sinh \left\{ \left[ \sqrt{\frac{v_0^2 \alpha^2 - (v_0^2 - a^2 l^2)}{(v_0^2 - a^2 l^2)^2}} \right] \xi \right\}, \quad (16)$$

as shown in Figure 3. Moreover in the special case of  $v_0^2 - a^2 l^2 = v_0^2 \alpha^2$ , the non-oscillatory solution degenerates to

$$u(\xi) = B \xi e^{-\xi / v_0 \alpha}, \quad (17)$$

as depicted in Figure 4. Note that  $A$  and  $B$  are constants that can always be assigned arbitrary values. Finally for  $v_0^2 - a^2 l^2 > v_0^2 \alpha^2$ , we obtain solutions in the oscillatory regime given by

$$u(\xi) = e^{-v_0 \alpha \xi / v_0^2 - a^2 l^2} [C_1 \exp(i \Omega \xi) + C_2 \exp(-i \Omega \xi)], \quad (18)$$

where  $\Omega = \sqrt{\frac{v_0^2 (1 - \alpha^2) - a^2 l^2}{(v_0^2 - a^2 l^2)^2}}$ . Solution (18) is valid in the region described by the parabolic equation:  $\alpha^2 + \frac{a^2 l^2}{v_0^2} = 1$ ,

which gives  $\alpha = 0$ , when  $a^2 l^2 = v_0^2$ , and  $a^2 l^2 = 0$ , when  $\alpha = 1$ , as depicted in Figure 5; where the region of the oscillatory solution regime is highlighted.

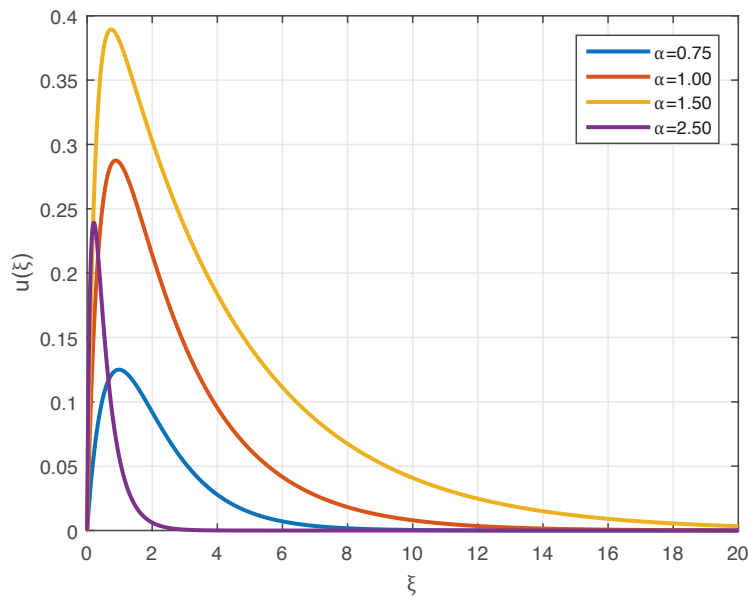


**Figure 3.** Non-oscillatory solution (16) that mimics a stick-slip motion. This is for  $A = 1.00$ ,  $a^2 l^2 = 1.00$ ,  $v_0^2 = 2.00$  and variation of  $\alpha$  parameter.

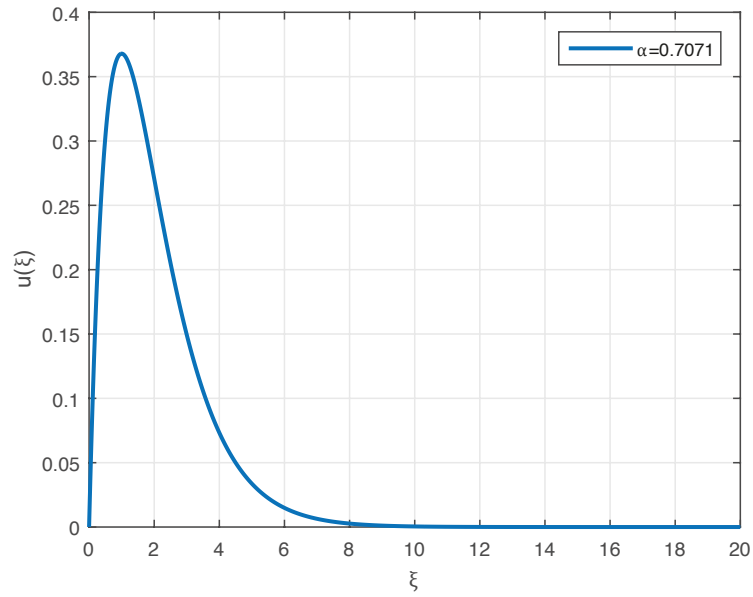


**Figure 4.** Non-oscillatory solution (17) that mimics a stick-slip motion. This is for  $B = 1.00, a^2l^2 = 1.00, v_0^2 = 2.00$  and  $\alpha = 1/\sqrt{2}$ .

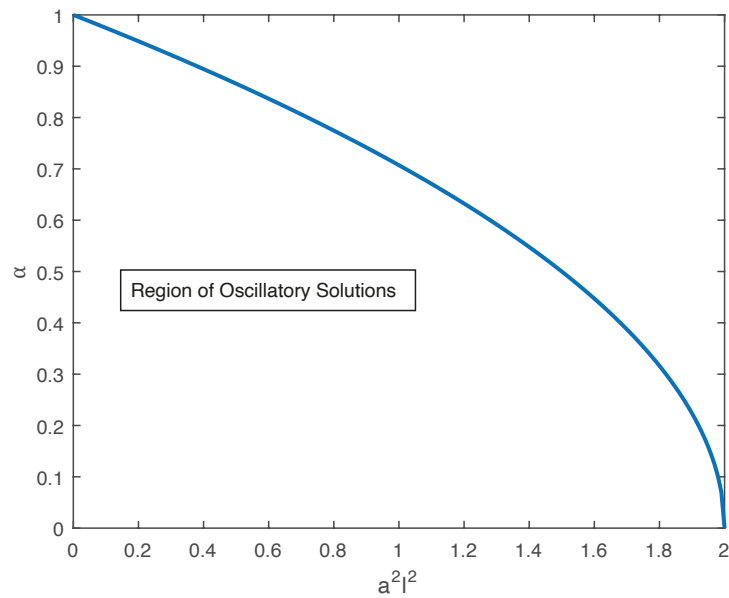


**Figure 5.** Region of oscillatory solution (18), defined by the parabolic equation:  $\alpha^2 + \frac{a^2l^2}{v_0^2} = 1$ . This is for  $v_0^2 = 2.00$  and underscores the crucial role played by the  $\alpha$  parameter.

The velocity of the system is  $v(\xi) = \frac{du(\xi)}{d\xi} = \left[ \frac{-v_0\alpha}{(v_0^2 - a^2l^2)} \right] \times e^{-\frac{v_0\alpha\xi}{(v_0^2 - a^2l^2)}} [C_1 \exp(i\Omega\xi) + C_2 \exp(-i\Omega\xi)] + [i\Omega] \times e^{-\frac{v_0\alpha\xi}{(v_0^2 - a^2l^2)}} [C_1 \exp(i\Omega\xi) - C_2 \exp(-i\Omega\xi)]$ ; where the region of the The condition that the initial velocity is  $v_0$  coupled with the initial displacement being zero, helps us to re-write solution (18) in the form

$$u(\xi) = v_0\Omega^{-1} e^{-v_0\alpha\xi/(v_0^2 - a^2l^2)} \sin(\Omega\xi), \tag{19}$$

## Generation of rogue wave in an earthquake fault

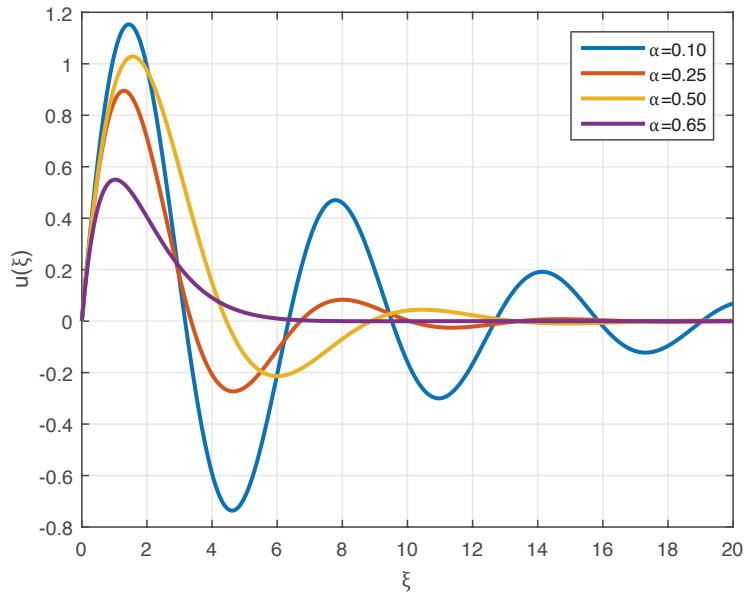


**Figure 6.** Damped oscillatory displacement (19), for  $a^2 l^2 = 1.00$ ,  $v_0^2 = 2.00$  and variation of  $\alpha$  parameter.

as depicted in Figure 6. It is important to note that  $v_0 \Omega^{-1}$  denotes the amplitude of displacement in solution (19), with this displacement  $u(\xi)$  increases with  $\xi$ , reaches the peak value and then decreases with  $\xi$ . The peak value of  $u(\xi)$  occurs at  $\xi_p = \Omega^{-1} \tan^{-1}[\Omega(v_0^2 - a^2 l^2)/v_0 \alpha]$  and the corresponding oscillatory velocity profile given in Figure 7.

Most vibrations occur at faults where tectonic plates converge, diverge, or slide past each other. Although the plates move steadily, their boundaries are often constraint to stick-slip motion as shown in Figure 3 and Figure 4. The nature of the frictional forces between the tectonic plates is inextricably linked to the  $\alpha$  parameter; which greatly controls the dynamics of the stick-slip motion and the magnitude of the hazard caused by the earthquake tremor [Decanini and Mollaioli, 1998]. We observe that for fixed values of  $a^2 l^2$  as shown in Figure 5, the region of observing stick-slip motion increases with increase in the values of the  $\alpha$  parameter. On the other hand, small values of  $\alpha$  parameter causes the stick-slip motion to evolve into a damped oscillatory motion as shown in Figure 6; with the corresponding velocity profile of the motion given in Figure 7. It is equally observed that as values of the

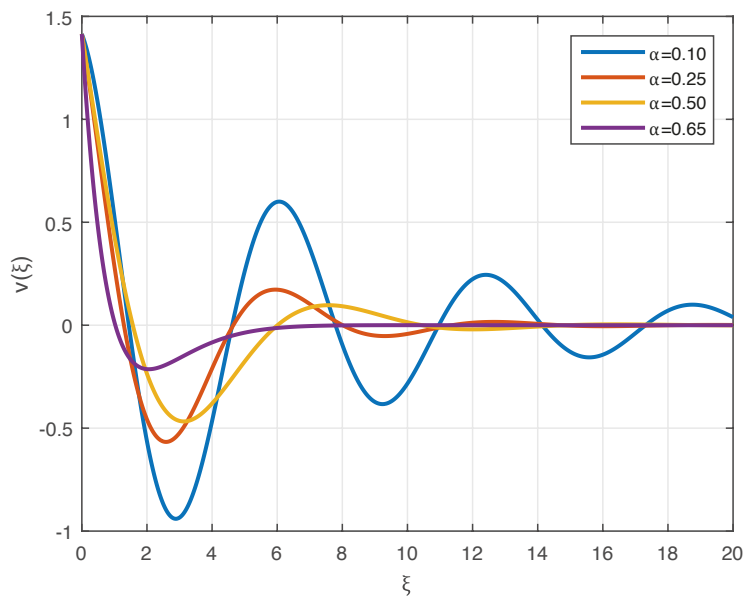


**Figure 7.** Corresponding velocity profile of the damped oscillatory displacement given in Figure 6.

$\alpha$  parameter is gradually increased within a range, the oscillatory motion in Figure 6 slowly dies down and may be locked (i.e. do not oscillate most of the time especially for  $\alpha = 0.65$ ). The stick-slip and damped oscillatory motions occur frequently along earthquake faults, but cannot always be felt on a larger scale because of the low amplitude of oscillations that typically characterize the linear system.

#### 4. Nonlinear wave dynamics in subduction zones

Subduction is a lithospheric process which occurs at meeting point of tectonic plate boundaries. Generally one plate under thrusts the other and eventually sinks into the earth mantle [Lallemand, 2014]. Subduction zones are generally associated with large earthquakes and active volcanoes, and can mostly be identified both on earth surface and oceanic plates. The tectonic regime of the upper plate of a subduction zone is dictated by the interactions between the plates at their common interface of convergence. Also, the type of coupling between tectonic plates at subduction zones is inextricably linked to the magnitude of the seismic hazard induced [Brune, 1968; Davies and Brune, 1971]. In the last decades, GPS stations are increasingly being used to monitor subduction zones in order to give a better estimate of tectonic plate couplings and hence a more realistic picture of the nonlinear dynamics that characterize these zones [Scholz and Campos, 2012; Chemenda et al., 2000; Shemenda, 1992].

We now focus on high degree of oceanic inter plate coupling at subduction zones in which  $\gamma \neq 0$  [Nkomom et al., 2021; Akishin et al., 2000; Pelap et al., 2016]. Consequently we consider small amplitude oscillation wave solution to equation (10), by employing the multiple-scale method [Remoissenet, 1986; Nfor et al., 2021; Nfor, 2021; Nfor et al., 2018; Nfor and Mokoli, 2016]. We initially introduce the change of variable

$$u(x, t) = \varepsilon \rho(x, t), \quad (20)$$

where  $\varepsilon$  is a small parameter (i.e.  $\varepsilon \ll 1$ ). Furthermore in a regime of weak frictional force between tectonic plates  $\alpha \rightarrow \varepsilon^2 \alpha$ ; this transform equation (10) to

$$\ddot{\rho} = c_0^2 \frac{\partial^2 \rho}{\partial x^2} - (1 + \varepsilon^2 \gamma \rho^2) \rho + 2\varepsilon^2 \alpha \dot{\rho}, \quad (21)$$

where  $c_0^2 = a^2 l^2$ .

Modulated wave solutions of equation (21) is then considered of the form

$$\rho(x, t) = \Psi e^{i(kx - \omega t)} + \Psi^* e^{-i(kx - \omega t)}, \quad (22)$$

where (\*) stands for complex conjugate,  $k$  is the wave vector, and  $\omega$  is the frequency. The main equation of motion describing the dynamics of the system is the one for which the function  $\Psi e^{i(kx - \omega t)}$  is the soliton solution, hence the amplitude will be considered slowly changing in space and time. Therefore, this amplitude is treated as functions of the new space and time scales  $X_i = \varepsilon^i x$  and  $T_i = \varepsilon^i t$  respectively [Remoissenet, 1986; Nfor et al., 2021; Nfor, 2021].

Thus, the solution  $u(x, t) = \sum_{i=0}^{\infty} \varepsilon^i \rho_i(X_0, X_1, X_2, \dots, T_0, T_1, T_2)$  and the derivative operators  $\frac{\partial}{\partial t}$  and  $\frac{\partial}{\partial x}$  are expanded as

$$\frac{\partial}{\partial t} = \frac{\partial}{\partial T_0} + \varepsilon \frac{\partial}{\partial T_1} + \varepsilon^2 \frac{\partial}{\partial T_2} + O(\varepsilon^3), \quad (23)$$

$$\frac{\partial}{\partial x} = \frac{\partial}{\partial X_0} + \varepsilon \frac{\partial}{\partial X_1} + \varepsilon^2 \frac{\partial}{\partial X_2} + O(\varepsilon^3). \quad (24)$$

## Generation of rogue wave in an earthquake fault

In this light we set  $\Psi(x, t) = \Psi(X_1, T_1), \exp[i(kx - \omega t)] = \exp[i(kX_0 - \omega T_0)]$  and by substituting equations (22), (23), and (24) into the low-amplitude equation (21) and grouping all first harmonic terms together give

$$-\omega^2\Psi - 2i\varepsilon\omega\Psi_{T_1} + \varepsilon^2\Psi_{T_1T_1} - c_0^2[-k^2\Psi + 2i\varepsilon k\Psi_{X_1} + \varepsilon^2\Psi_{X_1X_1}] + \Psi + 3\varepsilon^2\gamma|\Psi|^2\Psi = -2i\varepsilon^2\alpha\omega\Psi. \quad (25)$$

Terms independent of  $\varepsilon$  in equation (25) yields the dispersion relation

$$\omega^2 = 1 + c_0^2k^2, \quad (26)$$

with group velocity  $v_g = \frac{kc_0^2}{\omega}$ . By considering the new coordinate system

$$y = X_1 - v_g T_1, \quad \tau = \varepsilon T_1, \quad (27)$$

with terms of order  $\varepsilon^2$  equation (25) is reduced to

$$i\frac{\partial\Psi}{\partial\tau} - P\frac{\partial^2\Psi}{\partial y^2} - Q|\Psi|^2\Psi = i\alpha\Psi. \quad (28)$$

The coefficients  $P$  and  $Q$  are functions of  $k$ , and are given by

$$P = \frac{v_g^2 - c_0^2}{2\omega}, \quad (29a)$$

$$Q = \frac{\gamma}{2\omega}. \quad (29b)$$

Note that for  $\alpha > 0$  equation (28) is known as the forced Nonlinear Schrodinger (NLS) equation, while we have damped NLS equation for  $\alpha < 0$ . Equation (28) has a broad spectrum of applications in continuum mechanics, plasma physics, nonlinear optics, and neural networks [Achu et al., 2018a; Achu et al., 2018b]. For  $PQ > 0$ , the system of equation (28) readily admits stable envelope soliton solution with vanishing amplitude as  $|y| \rightarrow \infty$  which corresponds to a myriad of bright solitary wave profiles. However for  $PQ < 0$ , propagation of stable plane waves or dark solitons are identified. We note that for small  $k$  values, the dispersion coefficient  $P$  is always negative and the coupling between two tectonic plates in the earth crust is best modelled as a softening spring (i.e.  $\gamma < 0$ ). Hence we naturally work in the positive range of  $PQ$ , where approximate large amplitude oscillations (rogue wave solutions) of equation. (28) can be obtained.

### 4.1 Evolution of rogue waves

Rogue waves are giant waves which suddenly appear and disappear on sea surfaces. Such waves are characterized by very large-amplitude, accompanied by deep troughs, which occur before and/or after the largest crest [Kharif et al., 2009; Dysthe et al., 2008; Adcock and Taylor, 2014; Nikolkina and Didenkulova, 2014; Mori et al. 2002]. It should be noted that frictional forces across the surface of fault or subduction zones holds rocks together in the earth crust (or oceanic plates) and resists external perturbations. When enough stress has built up within the fault or subduction zones, the rocks slip suddenly thus releasing energy in form of waves traveling through the rocks. The aim of this subsection is to investigate on the propagation of these waves in subduction zones that sometimes evolve into rogue waves. The violent shaking observed during earthquakes is inextricably linked to the generation of these rogue waves, which carries huge amount of energy by virtue of its large amplitude.

Since equation (28) is non-integrable, different analytic methods have been employed to obtain appropriate solutions in different physical context [Achu et al., 2018a; Achu et al., 2018b]. By considering the transformation  $\Psi(y, \tau) = e^{\alpha\tau} \sqrt{\sigma(\tau)} \exp[i(\alpha\sigma(\tau)y^2)/2P] \psi(Y\Gamma)$ , we Taylor expand the exponential term  $e^{\alpha\tau}$  in the limit  $|\alpha\tau| \ll 1$ , and re-write equation (28) as [Onorato and Proment, 2012]

$$i \frac{\partial \psi}{\partial \Gamma} - P \frac{\partial^2 \psi}{\partial Y^2} - Q |\psi|^2 \psi = 0, \quad (30)$$

where  $\sigma(\tau) = \frac{1}{1 - 2\alpha\tau}$ ,  $Y(y, \tau) = \sigma(\tau)y$  and  $\Gamma(\tau) = \sigma(\tau)\tau$ . The Peregrine or rational solution to equation (30) is given by [Peregrine, 1983; Onorato et al., 2013]

$$\psi(Y, \Gamma) = \psi_0 \exp(-iQ\psi_0^2\Gamma) \left[ \frac{4P(1 - i2Q\psi_0^2\Gamma)}{P + P(2Q\psi_0^2\Gamma)^2 + 2Q\psi_0^2Y^2} - 1 \right], \quad (31)$$

which can easily be transformed back to the  $(y, \tau)$  coordinate system to read [Onorato and Proment, 2012]

$$\begin{aligned} \Psi(y, \tau) = \Psi_0 e^{\alpha\tau} \sqrt{\sigma(\tau)} & \left\{ \frac{[4P - [P + P(2Q\Psi_0^2\sigma(\tau)\tau)^2 + 2Q\Psi_0^2(\sigma(\tau)y)^2]] \cos \Omega_1 + [8PQ\Psi_0^2\sigma(\tau)\tau] \sin \Omega_1}{P + P(2Q\Psi_0^2\sigma(\tau)\tau)^2 + 2Q\Psi_0^2(\sigma(\tau)y)^2} \right\} + \\ & i\Psi_0 e^{\alpha\tau} \sqrt{\sigma(\tau)} \left\{ \frac{[4P - [P + P(2Q\Psi_0^2\sigma(\tau)\tau)^2 + 2Q\Psi_0^2(\sigma(\tau)y)^2]] \sin \Omega_1 - [8PQ\Psi_0^2\sigma(\tau)\tau] \cos \Omega_1}{P + P(2Q\Psi_0^2\sigma(\tau)\tau)^2 + 2Q\Psi_0^2(\sigma(\tau)y)^2} \right\}, \end{aligned} \quad (32)$$

where

$$\Omega_1 = \frac{\alpha\sigma(\tau)y^2}{2P} - Q\Psi_0^2\sigma(\tau)\tau. \quad (33)$$

The spatial and temporal localization profiles of solution (32) are depicted in Figure 8, Figure 9, and Figure 10 as the parameter  $\alpha$  is varied. In fact, the solution generally describes the amplification of an initial infinitesimal disturbance of a plane wave in which the maximum amplitude can reach three times that of the initial wave amplitude. It has the ability of appearing from nowhere and then disappearing without a residual trace. The nonlinearity introduced by the softening springs has given us the unique opportunity to observe the so-called Peregrine solitons (or breathers), which are waves characterized by an abnormally high peak which is sandwiched by depressions. Some intrinsic features of these Peregrine solitons are used to explain the mechanism of rogue wave formation. In the context of marine environment as shown in Figure 8, Figure 9, and Figure 10, a rogue wave would appear as a sudden fluid pressure spike that trigger ultimate seismic moment release in subduction zones.

This classical rogue wave soliton solution (32) features a self-focusing wave that appears from low background oscillations for  $\tau < 0$  and suddenly reaches a peak at the epicenter ( $y = 0, \tau = 0$ ); and vanishes quickly into the background noise. Furthermore as the parameter  $\alpha$  is varied, the amplitude of background plane wave solution is also altered. For example in a dissipative medium as in Figure 8 for  $\alpha = -0.01$ , the background plane waves gradually diminishes as time evolves. For a non-dissipative medium (i.e.  $\alpha = 0.00$ ) as in Figure 9, we observe constant background plane waves. Finally in a forcing medium for which  $\alpha > 0$ , there is a steady increase in the amplitude of the background plane waves as in Figure 10 for  $\alpha = 0.01$ .

Solution (20) can now be written more appropriately as

$$\begin{aligned} u(x, t) = 2\epsilon e^{\alpha\tau} \sqrt{\sigma(\tau)} & \left\{ \frac{[4P - [P + P(2Q\Psi_0^2\sigma(\tau)\tau)^2 + 2Q\Psi_0^2(\sigma(\tau)\epsilon x)^2]] \cos \Omega_2 + [8PQ\Psi_0^2\sigma(\tau)\tau] \sin \Omega_2}{P + P(2Q\Psi_0^2\sigma(\tau)\tau)^2 + 2Q\Psi_0^2(\sigma(\tau)\epsilon x)^2} \right\} \cos(kx - \omega t) - \\ & \left\{ \frac{[4P - [P + P(2Q\Psi_0^2\sigma(\tau)\tau)^2 + 2Q\Psi_0^2(\sigma(\tau)\epsilon x)^2]] \sin \Omega_2 - [8PQ\Psi_0^2\sigma(\tau)\tau] \cos \Omega_2}{P + P(2Q\Psi_0^2\sigma(\tau)\tau)^2 + 2Q\Psi_0^2(\sigma(\tau)\epsilon x)^2} \right\} \sin(kx - \omega t), \end{aligned} \quad (34)$$

where

$$\Omega_2 = \frac{\alpha\sigma(\tau)\varepsilon^2x^2}{2P} - Q\Psi_0^2\sigma(\tau)\tau, \quad \sigma(\tau) = \frac{1}{1-2\alpha\varepsilon^2t}, \quad \tau = \varepsilon^2t. \quad (35)$$

The spatio-temporal evolution of the rogue wave solution (34) shown in Figure 11, clearly matches with an earthquake profile that emanates from the epicentre located at the origin (0, 0). Epicentres are generally located around faults or subduction zones; which are regions where tectonic plates moves laterally with respect to each other as clearly captured by the modified BK model of earthquake phenomena highlighted above. Note that seismology is a scientific discipline that generally deals with the propagation of this large amplitude waves in the earth crust, leading to violent vibrations that causes enormous destruction. When the frictional forces between the tectonic plates along an earthquake fault are varied, the rogue waves evolve differently. For example for  $\alpha = -0.01$  as in

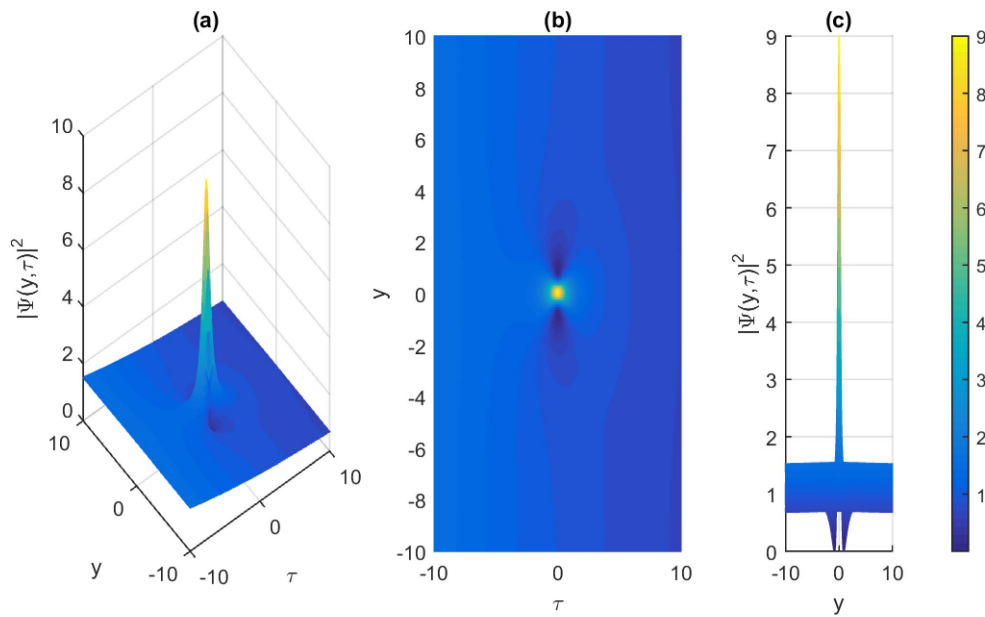


**Figure 8.** Rogue wave evolution in 3D and 2D representation of the intensity  $|\Psi(y, \tau)|^2$  for solution (32). This is for  $\alpha = 1.00, l = 1.50, k = 0.56, \gamma = -0.87, \Psi_0 = 1.00$ , and  $\alpha = -0.01$ .

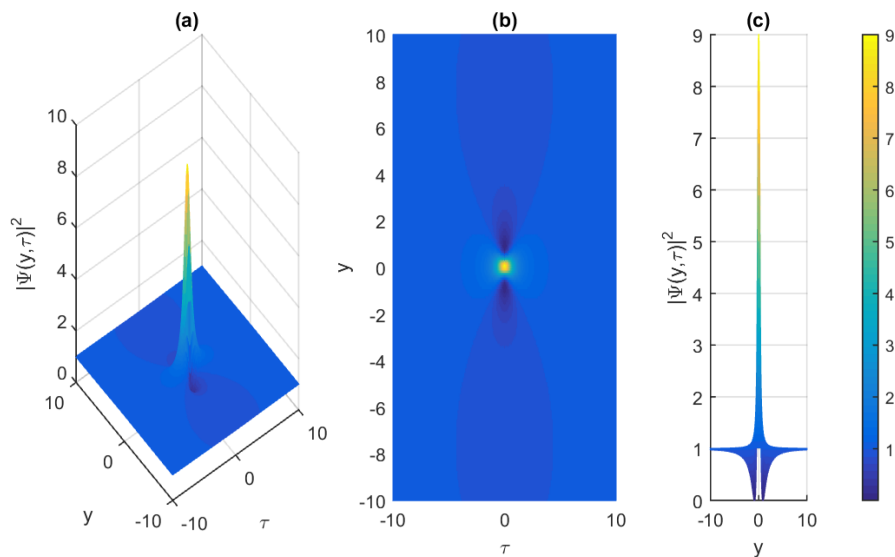


**Figure 9.** Parameters are the same as in Figure 8, but for  $\alpha = 0.00$ .

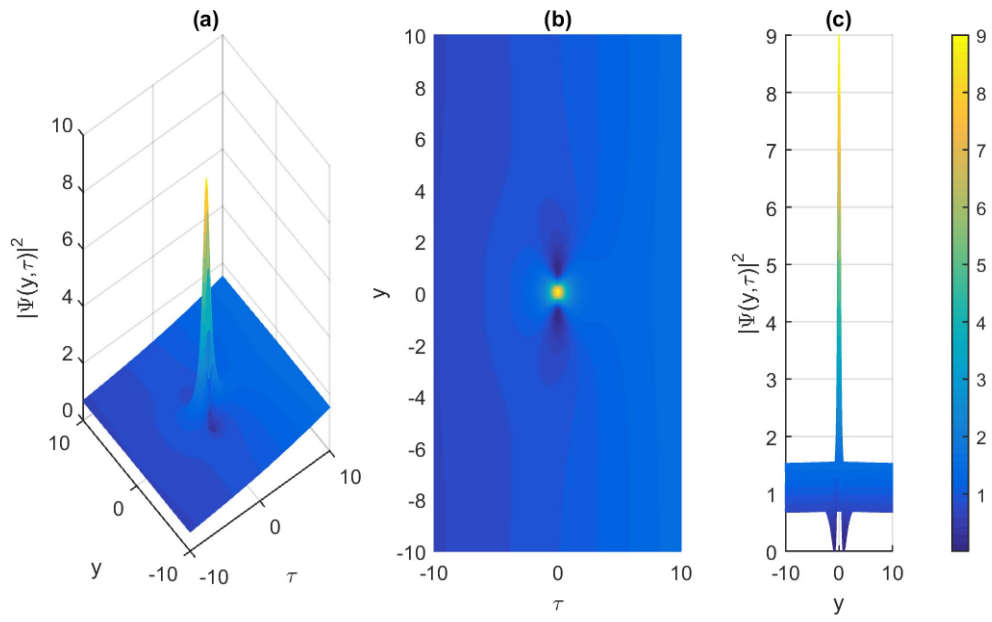


Figure 10. Parameters are the same as in Figure 8, but for  $\alpha = 0.01$ .

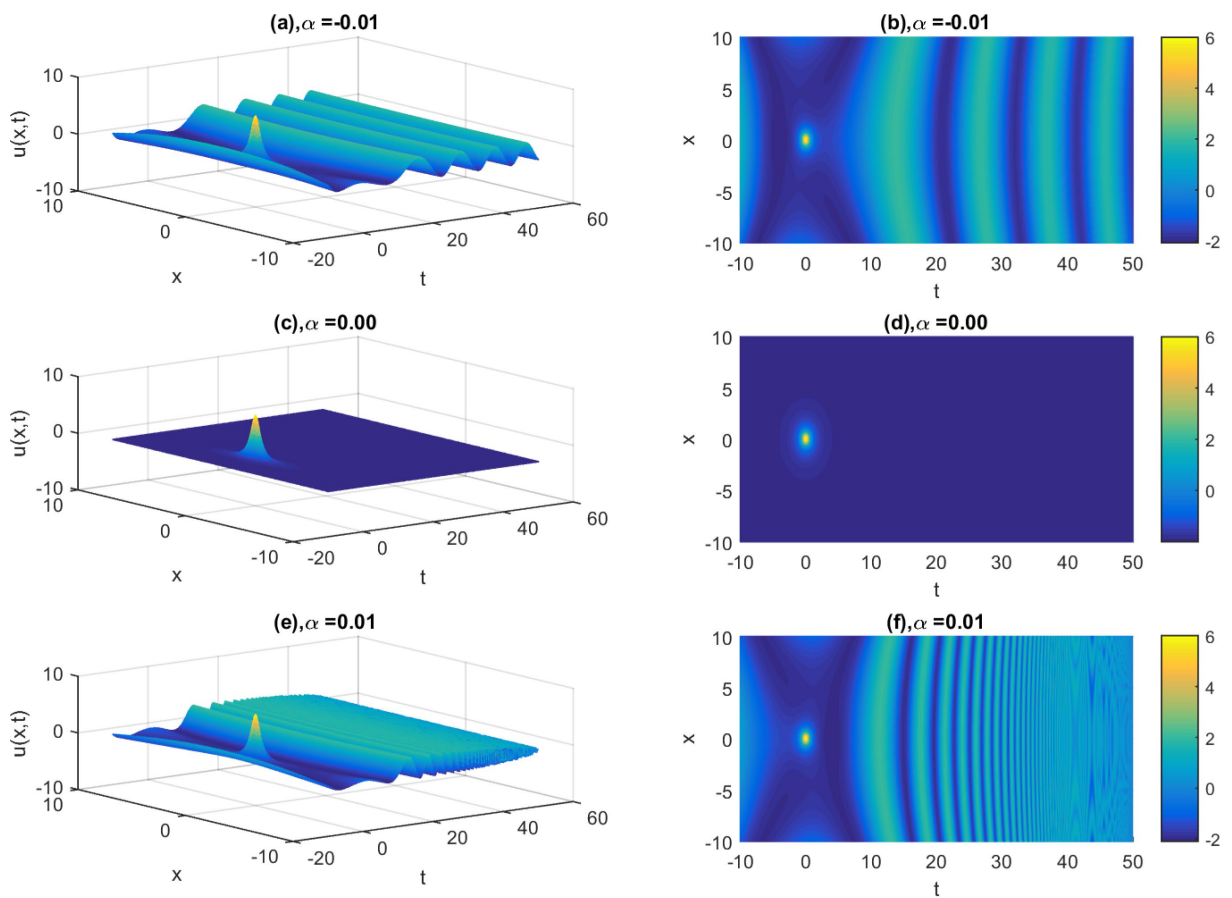
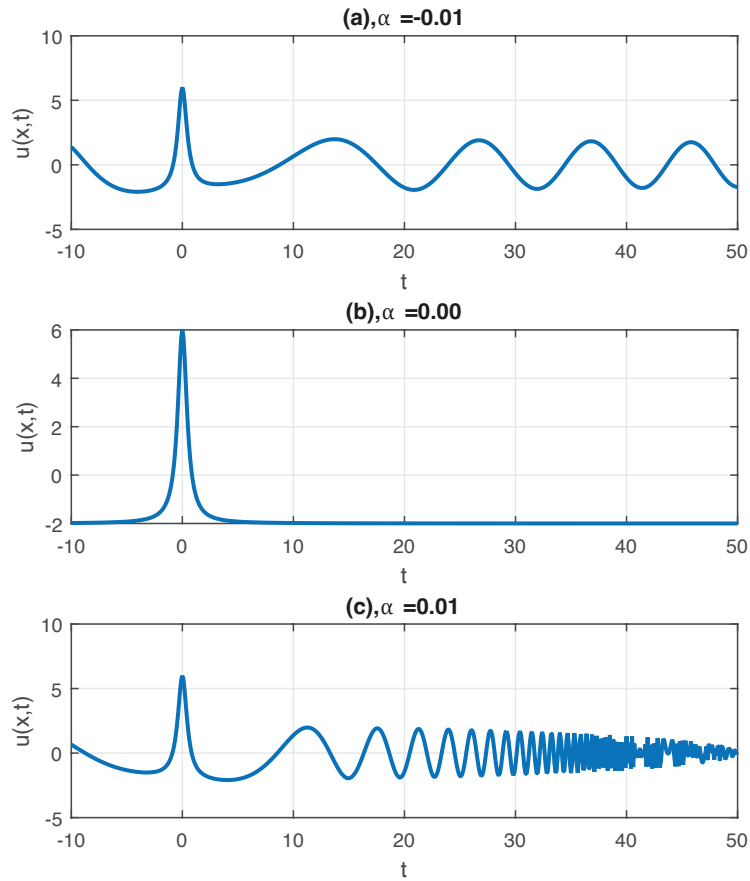


Figure 11. Profile of solution (34) that depicts the spatio-temporal evolution of rogue waves. This induces earthquake with the epicentre at the origin. This is for the parameters  $a = 1.00, l = 1.00, k = 0.00, \gamma = -0.67, \Psi_0 = 1.00, \omega^2 = 1.00, \varepsilon = 1.00$ , and  $\alpha$  is varied.

## Generation of rogue wave in an earthquake fault



**Figure 12.** Time series dynamics at the epicentre ( $x = 0.00$ ), with the same parameters as in Figure 11.

Figure 11(a,b), the huge wave amplitude at the epicentre drastically reduces and metamorphosis into plane waves as time passes after the earthquake tremor.

The classical profile of a rogue wave is clearly manifested in Figure 11(c,d), where there is zero frictional forces between tectonic plates (i.e.  $\alpha = 0.00$ ). In this case, the very large amplitude disturbance at the epicentre quickly disappears without any trace, leaving behind huge material damage. Numerous accidents have also been recorded in sea navigation during encounters between big ships and these rogue waves. The origin of rogue waves is still a very controversial issue, with increasingly different theoretical as well as experimental approaches under development to elucidate on this complex phenomenon [Akhmediev and Pelinovsky, 2010]. A huge percentage of these rogue waves were initially observed around the Pacific and Atlantic oceans and Mediterranean sea, which are known regions of subduction zones. Hence it is becoming increasingly clear that these rogue waves emanates from the dynamics of modified Burridge-Knopoff model, as strongly suggested by the analytical result captured in Figure 11(c,d). For  $\alpha = 0.01$ , the rogue waves rapidly evolve into low amplitude plane waves away from the epicentre as shown in Figure 11(e,f). The time series dynamics at the epicentre is clearly shown in Figure 12 as the parameter  $\alpha$  is varied. Increasing the value of  $\alpha$  generally induces high frequency plane waves that proceed the violent vibrations at the epicentre, as highlighted in Figure 12(c). By virtue of the resistive medium of the oceanic subduction zones or earth crust, these vibrations naturally dies down as reflected in the corresponding time series dynamics in Figure 12(a) for  $\gamma = -0.01$ .

### 4.2 Numerical investigation

The aim of this subsection is to ascertain the ability of the modified one-dimensional BK equation in supporting the rogue wave solutions that was analytically obtained in the preceding subsection. This is a very important step because all the solutions obtained so far are approximations, based on the assumptions made in the analytical

calculations. For the purpose of this numerical analysis, we will integrate equation (4) using an explicit Runge-Kutta scheme. Prior to this integration, it is important to define the form of the frictional law by considering the approximation  $\Phi(2\alpha v + 2\alpha \dot{u}_n) \approx -2\alpha \dot{u}_n$  and rewrite equation (4) as

$$\ddot{u}_n = l^2(u_{n+1} - 2u_n + u_{n-1}) - (1 + \gamma u_n^2)u_n + 2\alpha \dot{u}_n. \quad (36)$$

In order to determine the outcome of the long term evolution of rogue waves, we have to numerically solve equation (36) by considering solution (34); which can be re-written in the discrete form

$$u_n(t) = 2\varepsilon\Psi_0 e^{\varepsilon^2 \alpha t} \sqrt{\sigma(t)} \left\{ \left[ \frac{4P - [P + P(2Q\Psi_0^2\sigma(t)\varepsilon^2 t)^2 + 2Q\Psi_0^2(\sigma(t)\varepsilon n a)^2]}{P + P(2Q\Psi_0^2\sigma(t)\varepsilon^2 t)^2 + 2Q\Psi_0^2(\sigma(t)\varepsilon n a)^2} \cos \Omega_{2n} + [8PQ\Psi_0^2\sigma(t)\varepsilon^2 t] \sin \Omega_{2n} \right] \times \right. \\ \left. \cos(kna - \omega t) - \left[ \frac{4P - [P + P(2Q\Psi_0^2\sigma(t)\varepsilon^2 t)^2 + 2Q\Psi_0^2(\sigma(t)\varepsilon n a)^2]}{P + P(2Q\Psi_0^2\sigma(t)\varepsilon^2 t)^2 + 2Q\Psi_0^2(\sigma(t)\varepsilon n a)^2} \sin \Omega_{2n} - [8PQ\Psi_0^2\sigma(t)\varepsilon^2 t] \cos \Omega_{2n} \right] \sin(kna - \omega t) \right\}, \quad (37)$$

where

$$\Omega_{2n} = \frac{\alpha\sigma(t)(\varepsilon n a)^2}{2P} - Q\Psi_0^2\sigma(t)\varepsilon^2 t, \quad \sigma(t) = \frac{1}{1 - 2\alpha\varepsilon^2 t}. \quad (38)$$

By setting  $t = 0$  in solution (37), we obtain the initial condition for our numerical scheme given by

$$u_n(t = 0) = \left\{ \frac{2\varepsilon\Psi_0[3P - 2Q(\Psi_0\varepsilon n a)^2]}{P + 2Q(\Psi_0\varepsilon n a)^2} \right\} \cos \left[ \frac{\alpha(\varepsilon n a)^2}{2P} + kna \right]. \quad (39)$$

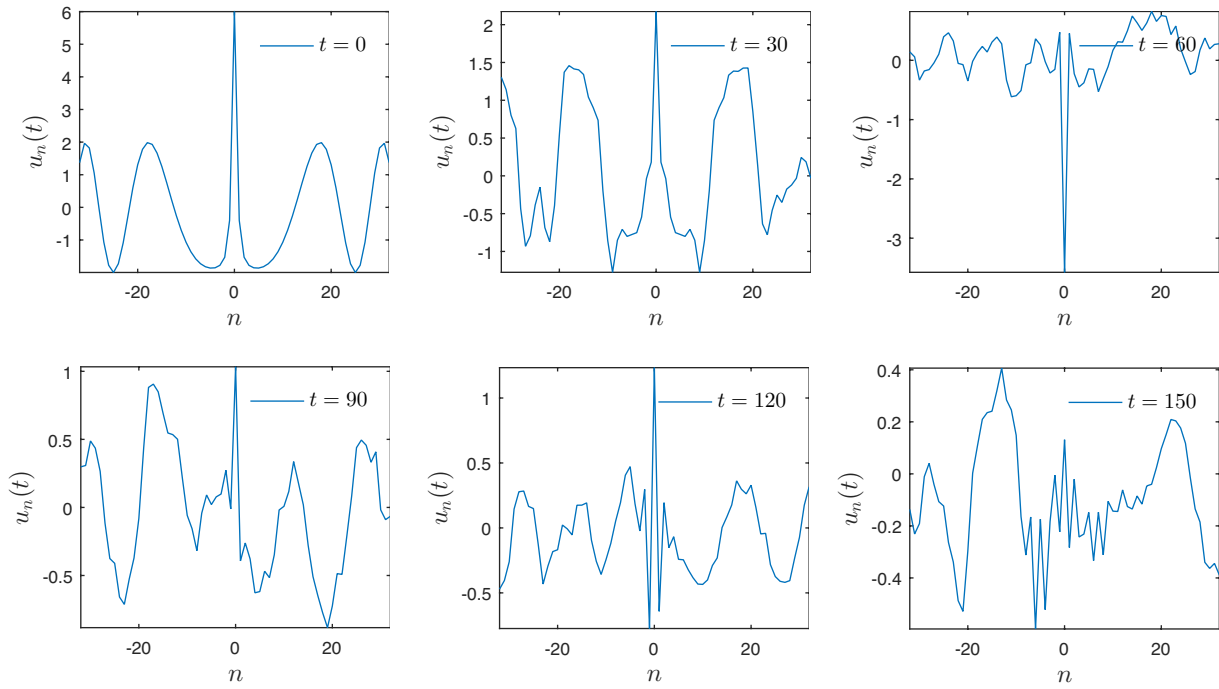
We then use the built-in MATLAB solver **ode45**, which is based on the fourth order Runge-Kutta formula. In fact it is a one-step solver, which means in computing  $u_n(t)$ ; it uses only the immediately preceding time point solution  $u_{n-t}(t)$ . Consequently, we obtain the various profiles of the rogue wave solution in Figure 13, Figure 14, and Figure 15 as the  $\alpha$  parameter is varied.

Figure 13 depicts the damped case in which  $\alpha = -0.01$ ; the initial height (at time  $t = 0$ ) of the wave profile at  $n = 0$  is about three times or more greater in every other point. The large amplitude wave gradually degenerates to low amplitude background plane waves as time evolves. As shown in Figure 14 for  $\alpha = 0.00$ , the system epitomizes all the characteristic of a rogue wave that initially appears at  $n = 0$  and disappears leaving behind very low amplitude oscillations. However a very interesting phenomenon occurs at  $t = 90$  in Figure 14; with the reappearance of these large amplitude waves and eventual disappearance without traces. The dynamics of the system is greatly modified for the forcing case in Figure 15 for  $\alpha = 0.01$ . We observe the sudden disappearance of this monster wave at  $t = 30$ , and the eventual reappearance with increasing amplitude as from  $t = 60$  to  $t = 120$  at the point  $n = 0$ . Additional wave peaks are equally observed at positions  $n = -20, -10$  at time  $t = 150$  in Figure 15. The forcing in the system (i.e.  $\alpha > 0$ ) may sometimes be induced by the flow of magma, after volcanic eruptions that naturally occurs in oceanic plates.

## 5. Conclusion

We have considered the dynamics of earthquake faults, whereby rogue waves are generated under varied conditions of frictional forces between tectonic plates in subduction zones. We exploited the modified one dimensional BK model in which the tectonic plates are linked together by softening and hardening springs. By using Newton's Laws of motion and exploiting the continuum limit approximation, we obtained the second order partial differential equation. Stick-slip and damped oscillatory motions are observed in the linear approximation, even though the effects are very minimal owing to the low amplitude of vibrations. By using the method of multiple scale expansion, the damped/forced nonlinear Schrodinger amplitude equation is obtained with its rogue wave solution that seems to give a satisfactory answer to the mechanism of generation of these oceanic monster waves.

## Generation of rogue wave in an earthquake fault



**Figure 13.** Evolution of rogue waves based on the numerical integration of discrete equation (36), with initial condition (39). This is for the parameters  $a = 1.00$ ,  $l = 1.00$ ,  $k = 0.00$ ,  $\gamma = -0.67$ ,  $\Psi_0 = 1.00$ ,  $\omega^2 = 1.00$ ,  $\varepsilon = 1.00$ , and  $\alpha = -0.01$ .

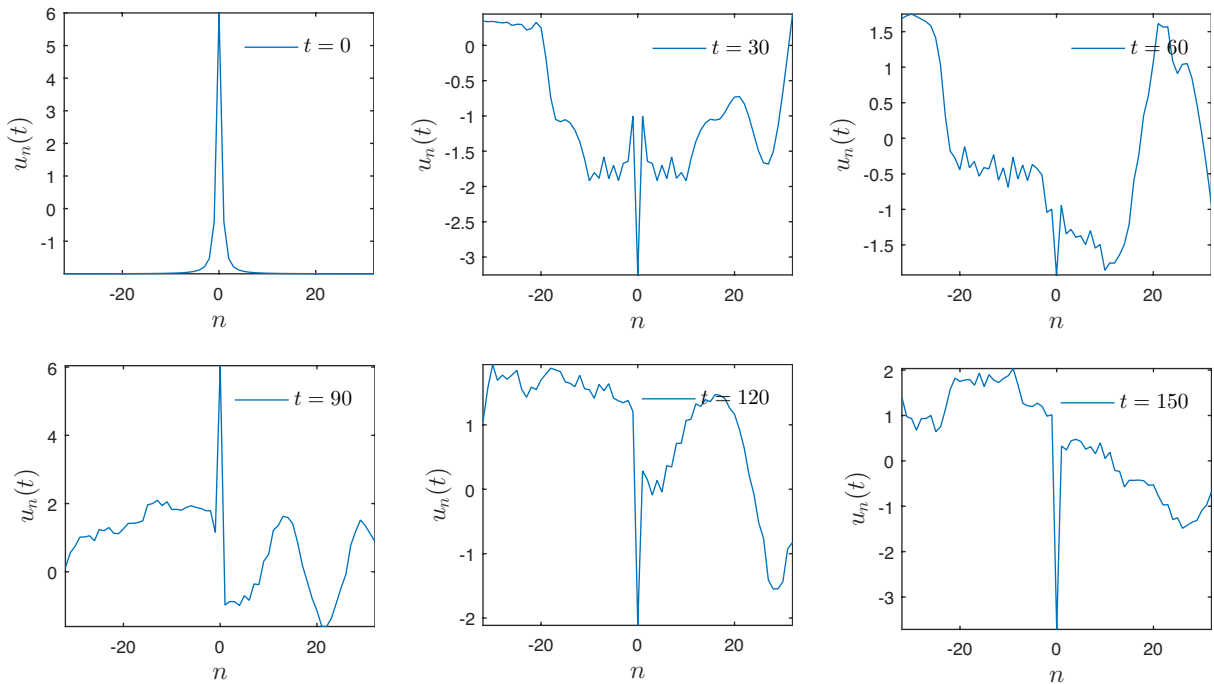


**Figure 14.** Rogue wave evolution with the same parameters as in Figure 13, but for  $\alpha = 0.00$ .

Ever since the observation of a monster wave on sea surfaces termed rogue waves, much work have been carried out to experimentally reproduce these large amplitude waves that appears from nowhere and suddenly disappears. Understanding the mechanisms of rogue wave formation would be an important step toward predicting their occurrence and devising means of mitigating their harmful effects. However the mechanism of rogue wave formation is still a very controversial issue because some scientists hold that its generation is as a result of linear interference, while others attribute it to a nonlinear phenomenon. By accepting the latter view point, rogue waves

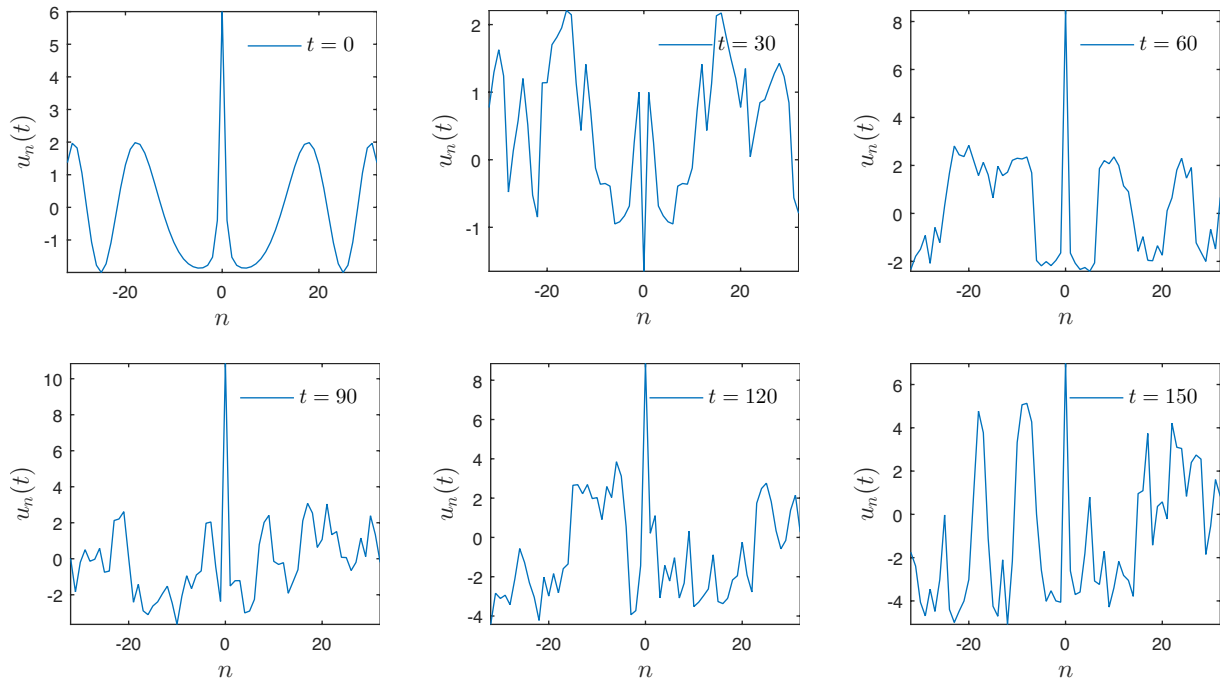


**Figure 15.** Rogue wave evolution with the same parameters as in Figure 13, but for  $\alpha = 0.01$ .

can be understood as the result of modulational instability that leads to the formation of large amplitude oscillating envelope solitons. In fact, we exploited the Peregrine soliton solution of the derived damped/forced nonlinear Schrodinger amplitude equation to explain why there is a sudden appearance and disappearance of large amplitude waves in oceans/seas that hosts subduction zones. The time series dynamics shows that this special prototype of freak wave generally evolves into low amplitude plane waves as observed in the linear regime.

We have thus derived the damped/forced NLS equation and presented the Peregrine soliton solution. These solutions are extreme short-wavelength standing wave, which is generated as a result of dispersive and nonlinear effects inherent in the tectonic plate system of earthquake fault. We propose here that rogue waves stemming from the dynamics of two nonlinearly coupled tectonic plates in subduction zones equally provide a source mechanism for earthquakes. We realize that our model is subject to improvement, but hope that our present results will enhance theoretical and experimental knowledge on rogue-like surface seismic waves in the context of maritime environment.

**Acknowledgements.** The authors are grateful for the financial assistance from the Cameroon Ministry of Higher Education, through the regular research grants to lecturers of state universities. N. Oma Nfor equally appreciates Dr. Tameh Jude of LaRAMaNS-University of Buea, for drawing the mechanical circuit diagram in Figure 1.

## References

- Achu, G. F., S. E. Mkam, F. M. Moukam Kakmeni and C. Tchawoua (2018a). Periodic soliton trains and informational code structures in an improved soliton model for biomembranes and nerves, *Phys. Rev. E*, 98, 022216.
- Achu, G. F., F. M. Moukam Kakmeni and A. M. Dikand'e (2018b). Breathing pulses in the damped-soliton model for nerves, *Phys. Rev. E*, 97, 012211.
- Adcock, T. A. A. and P. H. Taylor (2014). The physics of anomalous ('rogue') ocean waves, *Rep. Prog. Phys.*, 77, 105901.
- Akhmediev, N. and E. Pelinovsky (2010). Discussion and debate: Rogue waves – towards a unifying concept? *European Phys. J.-Spec. Topics*, 185, 1, 1-266.
- Akhmediev, N., B. Kibler, F. Baronio, M. Belic, W.-P. Zhong, Y. Zhang, W. Chang, J. M. Soto-Crespo, P. Vouzas, P. Grelu, et al. (2016). Roadmap on optical rogue waves and extreme events, *J. Opt.*, 18, 063001.

- Akishin, P. G., M. V. Altaisky, I. Antoniou, A. D. Budnik and V. V. Ivanov (2000). Burrige-Knopoff model and self-similarity, *Chaos solitons Fractals*, 11, 1-3, 207-222.
- Bailung, H., S. K. Sharma and Y. Nakamura (2011). Observation of Peregrine solitons in a multicomponent plasma with negative ions, *Phys. Rev. Lett.*, 107, 255005.
- Baro, J., A. Corral, X. Illa, A. Planes, E. Salje, W. Schranz, D. Soto-Parra and E. Vives (2013). Statistical similarity between the compression of a porous material and earthquakes, *Phys. Rev. Lett.*, 110, 088702.
- Ben-Zion, Y. and C. Sammis (2011). Brittle deformation of solid and granular materials with applications to mechanics of earthquakes and faults, *Pure Appl. Geophys.*, 168, 2147-2149.
- Brace, W. F. and J. D. Byerlee (1966). Stick-Slip as a mechanism for earthquakes, *Science*, 153, 990.
- Brune, J. (1968). Seismic moment, seismicity, and rate of slip along major fault zones, *J. Geophys. Res.*, 73, 777-784.
- Byerlee, J. D. (1970). The mechanics of stick-slip, *Tectonophysics*, 9, 475-486.
- Burrige, R. and L. Knopoff (1967). Model and theoretical seismicity, *Bull. Seismol. Soc. Am.*, 57, 341-371.
- Carlson, J. M. and J. Langer (1989a). Properties of earthquakes generated by fault dynamics, *Phys. Rev. Lett.*, 62, 2632.
- Carlson, J. M. and J. Langer (1989b). Mechanical model of an earthquake fault, *Phys. Rev. A*, 40, 6470-6484.
- Carlson, J. M., J. S. Langer, B. E. Shaw and C. Tang (1991). Intrinsic properties of a Burrige-Knopoff model of an earthquake fault, *Phys. Rev. A*, 44, 884-897.
- Carlson, J. M., J. S. Langer and B. E. Shaw (1994). Dynamics of earthquake faults, *Rev. Mod. Phys.*, 66, 657.
- Cartwright, J. H. E., V. M. Eguluz, E. Hernandez-Garcia and O. Piro (1999). Dynamics of elastic excitable media, *Int. J. Bif. Chaos*, 9, 2197-2202.
- Chemenda, A., S. Lallemand and A. Bokun (2000). Strain partitioning and inter-plate friction in oblique subduction zones: Constraints provided by experimental modeling, *J. Geophys. Res.*, 105(3), 5567-5581.
- Davies, G. and J. N. Brune (1971). Regional and global fault slip rates from seismicity, *Nature*, 229, 101-107.
- Decanini, L. D. and F. Mollaioli (1998). Formulation of elastic earthquake input energy spectra. *Earthquake Engineering and Structural Dynamics*, *Earthq. Eng. Struct. Dyn.*, 27(12), 1503-1522.
- Dudley J. M., F. Dias, M. Erkintalo and G. Genty (2014). Instabilities, breathers and rogue waves in optics, *Nat. Photonics*, 8, 755-764.
- Dysthe, K. B., H. E. Krogstad and P. Muller (2008). Oceanic rogue waves, *Ann. Rev. Fluid Mech.*, 40, 287-310.
- Enns, R. H. (2011). *It is a Nonlinear World*, New York: Springer.
- Estelle, T. D. D. and T. C. Kofane' (2015). Nonparaxial rogue waves in optical Kerr media, *Phys. Rev. E*, 91, 063201.
- Ganshin, A. N., V. B. Efimov, G. V. Kolmakov, L. P. Mezhev-Deglin and P. V. E. McClintock (2008). Observation of an inverse energy cascade in developed acoustic turbulence in superfluid Helium, *Phys. Rev. Lett.*, 101, 065303.
- Graham, D. M. (2000). NOAA vessel swamped by rogue wave, *Oceanspace*, 284.
- Hamiel, Y., V. Lyakhovskiy, S. Stanchits, G. Dresen and Y. Ben-Zion (2009). Brittle deformation and damage induced seismic wave anisotropy in rocks. *Geophysical Journal International*, 178, 901-909.
- Hohmann, R., U. Kuhl, H.-J. Stockmann, L. Kaplan and E. J. Heller (2010). Freak waves in the linear regime: a microwave study. *Phys. Rev. Lett.*, 104, 9, 093901.
- Kharif, C., E. Pelinovsky and A. Slunyaev (2009). *Rogue Waves in the Ocean*, 1st ed., Springer: Berlin, Germany.
- Kittel, C., W. D. Knight and M. A. Ruderman (1968). *Mechanics*, Berkeley Physics Course Volume 1, McGraw-Hill Book Co. New York N Y, 480.
- Lallemand, S. (2014). Active Continental Margin, *Encyclopedia of Marine Geosciences*, 103, 1-6.
- Langer, J. S., J. M. Carlson, R. M. Christopher and E. S. Bruce (1996). Slip complexity in dynamic models of earthquake faults, *Proc. Natl. Acad. Sci. USA*, 93, 3825-3829.
- Lawton, G. (2001). Monsters of the deep (the perfect wave), *New Scientist*, 170, 2297, 28-32.
- Main, I. (2013). Little earthquakes in the lab, *Physics*, 6, 20.
- Morales, J. E., G. James and A. Tonnelier (2018). Solitary waves in the excitable Burrige-Knopoff model, *Wave motion*, 76, 103-121.
- Mori, N., P. Liu and T. Yasuda (2002). Analysis of freak wave measurements in the Sea of Japan, *Ocean Engineering*, 29, 11, 1399-1414.
- Nfor, N. O. (2021). Higher order periodic base pairs opening in a finite stacking enthalpy DNA model, *J. Modern Phys.*, 12, 1843-1865.
- Nfor, N. O. and M. T. Mokoli (2016). Dynamics of nerve pulse propagation in a weakly dissipative myelinated axon, *J. Modern Phys.*, 7, 1166-1180.

- Nfor, N. O., P. G. Ghomsı and F. M. Moukam Kakmeni (2018). Dynamics of coupled mode solitons in bursting neural networks, *Phys. Rev. E*, 97, 022214.
- Nfor, N. O., S. B. Yamgou'e and F. M. Moukam Kakmeni (2021). Investigation of bright and dark solitons in  $\alpha$ ;  $\beta$ -Fermi Pasta Ulam lattice, *Chinese Phys. B*, 30, 020502.
- Nikolkina, I. and I. Didenkulova (2011). Rogue waves in 2006-2010, *Natural Hazards and Earth System Sciences*, 11, 2913-2924
- Nkomom, T. N., J. B. Okaly and A. Mvogo (2021). Dynamics of modulated waves and localized energy in a Burridge and Knopoff model of earthquake with velocity-dependant and hydrodynamics friction forces, *Physica A*, 583, 126283.
- Onorato, M. and D. Proment (2012). Approximate rogue wave solutions of the forced and damped nonlinear Schrödinger equation for water waves, *Phys. Lett. A*, 376, 3057-3059.
- Onorato, M., S. Residori, U. Bortolozzo, A. Montina and F. T. Arecchi (2013). Rogue waves and their generating mechanisms in different physical contexts, *Phys. Rep.*, 528, 47.
- Pelap, F. B., L. Y. Kagho and C. F. Fogang (2016). Chaotic behavior of earthquakes induced by a nonlinear magma up flow, *Chaos solitons Fractals*, 87, 71-83.
- Peregrine, D. (1983). Water waves, nonlinear Schrödinger equations and their solutions, *Journal of the Australian Mathematical Society Series*, 25, 1, 16.
- Remoissenet, M. (1986). Low-amplitude breather and envelope solitons in quasi-one-dimensional physical models, *Phys. Rev. B*, 33, 2386-2392.
- Scholz, C. H. and J. Campos (2012). The seismic coupling of subduction zones revisited, *Journal of Geophysical Research*, 117, B05310.
- Shats, M. and X. H. Punzmann (2010). Capillary rogue waves, *Phys. Rev. Lett.*, 104, 104503.
- Shemenda, A., (1992). *Subduction: Insights from Physical Modeling*, Netherlands: Kluwer Academic Publishers. in *Modern approaches in Geophysics*, 215 pp.
- Solli, D. R., C. Ropers, P. Koonath and B. Jalali (2007). Optical rogue waves, *Nature*, 450, 1054-1058.
- Wiggins, S., (1990). *Application to the Dynamics of the Damped Forced Duffing Oscillator: Introduction to Applied Nonlinear Dynamical Systems and Chaos*, New York: Springer-Verlag.
- Zhong, W.-P., M. Belic and B. A. Malomed (2015). Rogue waves in a two-component Manakov system with variable coefficients and an external potential, *Phys. Rev. E*, 92, 053201.

**\*CORRESPONDING AUTHOR: Nkeh OMA NFOR,**

Department of Physics, Higher Teacher Training College Bambili,  
The University of Bamenda, P. O. Box 39,  
Bambili-Cameroon  
e-mail: omnkeh@gmail.com